Geoscience Frontiers 4 (2013) 263–276

Contents lists available at SciVerse ScienceDirect

China University of Geosciences (Beijing)

Geoscience Frontiers

journal homepage: www.elsevier.com/locate/gsf

Research paper

Periodicities in the emplacement of large igneous provinces through the Phanerozoic: Relations to ocean chemistry and marine biodiversity evolution

Andreas Prokoph [a,*], Hafida El Bilali [b], Richard Ernst [b,c]

[a] Speedstat, 19 Langstrom Crescent, Ottawa, ON K1G 5J5, Canada
[b] Carleton University, Department of Earth Sciences, Herzberg Building, Ottawa, ON K1S 5B6, Canada
[c] ErnstGeosciences, 43 Margrave Avenue, Ottawa, ON K1T 3Y2, Canada

ARTICLE INFO

Article history:
Received 21 April 2012
Received in revised form
20 July 2012
Accepted 10 August 2012
Available online 25 August 2012

Keywords:
Large igneous provinces
Wavelet transform
Sulfur isotope
Mantle plume
Marine biodiversity
Periodicity

ABSTRACT

Large igneous provinces (LIPs) are considered a relevant cause for mass extinctions of marine life throughout Earth's history. Their flood basalts and associated intrusions can cause significant release of SO_4 and CO_2 and consequently, cause major environmental disruptions. Here, we reconstruct the long-term periodic pattern of LIP emplacement and its impact on ocean chemistry and biodiversity from $\delta^{34}S_{sulfate}$ of the last 520 Ma under particular consideration of the preservation limits of LIP records. A combination of cross-wavelet and other time-series analysis methods has been applied to quantify a potential chain of linkage between LIP emplacement periodicity, geochemical changes and the Phanerozoic marine genera record. We suggest a mantle plume cyclicity represented by LIP volumes (V) of $V = -(350–770) \times 10^3$ km^3 $\sin(2\pi t/170\text{ Ma}) + (300–650) \times 10^3$ km^3 $\sin(2\pi t/64.5\text{ Ma} + 2.3)$ for t = time in Ma. A shift from the 64.5 Ma to a weaker ~28–35 Ma LIP cyclicity during the Jurassic contributes together with probably independent changes in the marine sulfur cycle to less ocean anoxia, and a general stabilization of ocean chemistry and increasing marine biodiversity throughout the last ~135 Ma. The LIP cycle pattern is coherent with marine biodiversity fluctuations corresponding to a reduction of marine biodiversity of ~120 genera/Ma at ~600×10^3 km^3 LIP eruption volume. The 62–65 Ma LIP cycle pattern as well as excursion in $\delta^{34}S_{sulfate}$ and marine genera reduction suggest a not-yet identified found LIP event at ~440–450 Ma.

1. Introduction

Flood basalts and their associated plumbing systems represent large igneous provinces (LIPs) and are typically linked to mantle plumes that originate from deep in the mantle (e.g., Coffin and Eldholm, 1994; Ernst and Buchan, 2001; Courtillot et al., 2003) triggering large volume gas release in the ocean-atmospheric systems. Numerous studies have attempted to explore the links between the type, duration and magnitude of specific LIPs and temporally associated environmental perturbations (e.g., Caldeira and Rampino, 1993; Wignall, 2001; Berner, 2002; Svensen et al., 2009). In addition, there have also been evaluation of a long-term statistical link between the cycle of LIPs, ocean chemistry and biodiversity over the last 230 Ma and purely based on coeval timing of events (e.g., Caldeira and Rampino, 1993). A timing link between LIPs and mass extinctions has been discussed for several decades (e.g., Wignall, 2001; Courtillot and Renne, 2003), with ongoing high-resolution studies complementing this relationship (e.g., Isozaki, 2009; Saunders and Reichow, 2009). A recently discovered ~62 Ma and ~140 Ma cyclicity in the complete Phanerozoic marine fossil record (Rhode and Muller, 2005) has re-ignited the quest for primary and secondary geological factors might have caused these repeated fluctuations. For example, the ~62 Ma cyclicity in LIP, $^{87}Sr/^{86}Sr$ and $\delta^{34}S_{sulfate}$ records detected in independent studies (Prokoph et al., 2004a, 2008) have been merged to explain such patterns and possible relationships between these cycles (Melott et al., 2012).

* Corresponding author.
E-mail addresses: aprokocon@aol.com (A. Prokoph), elbilalihaf@hotmail.com (H. El Bilali), Richard.Ernst@ErnstGeosciences.com (R. Ernst).

Peer-review under responsibility of China University of Geosciences (Beijing).

Production and hosting by Elsevier

1674-9871/$ – see front matter © 2013, China University of Geosciences (Beijing) and Peking University. Production and hosting by Elsevier B.V. All rights reserved.
http://dx.doi.org/10.1016/j.gsf.2012.08.001

Here we attempt to reconstruct potential links between large-scale magmatism, ocean chemistry and biological evolution based on new databases and, for the first time, using cross-wavelet analysis to trace the cycles and their coherency though time and detect abrupt and gradual change. We used marine isotope records of sulfur and strontium as potentially continuous proxies for variability of igneous magmatism, in particular mantle plume related LIP eruptions. Moreover we used LIP volumes to better quantify magnitude relationships between LIP, oceanic chemistry and marine biodiversity evolution. The main challenging feature of the LIP record is its incompleteness. The LIP database is frequently updated with new LIPs being recognized as well as improvements in the ages, areal and volume extent of known LIPs (e.g., Torsvik et al., 2008; Reichow et al., 2009; Bryan et al., 2010; Ernst and Bleeker, 2010). However, the best dated and defined group of LIPs called "A10" (Ernst and Buchan, 2001) through the last 520 Ma have not changed or amended except for an increase in the ages of some LIPs dated only by the Ar/Ar method. The astronomical cycle based calibration of Fish Canyon sanidine reduced the $^{40}Ar/^{39}Ar$ method's absolute uncertainty from ~2.5% to 0.25%, and more importantly increased the absolute age of $^{40}Ar/^{39}Ar$-based dates by ~0.6% (Kuiper et al., 2008). In this way, the age-determination issues around the Permian–Triassic boundary are an exception. Considering the age uncertainties mentioned above and the biostratigraphic resolution to which fossil and geochemical records are fitted (e.g., Prokoph et al., 2008) the LIP records can be used for statistical robust comparison with other long-term geological records at ±2 Ma resolution. However, the A10-record does not include information on the size of the LIP, thus cannot provide a link between the magnitudes of an LIP and environmental changes.

2. Datasets and their compilation

For our study, we used updated databases of probability-weighted LIP initiation ages and volumes (Ernst and Buchan, 2001; Courtillot and Renne, 2003), $\delta^{34}S_{sulfate}$ (Kampschulte and Strauss, 2004; Paytan et al., 2004) and $^{87}Sr/^{86}Sr$ (Prokoph et al., 2008), and marine biodiversity (Sepkoski, 2002; Rhode and Muller, 2005) for the last 520 Ma with reference to the GTS2004 time scale (Gradstein et al., 2005). The LIP volume dataset has two versions. Version #1 uses the minimal value for volume ranges and also reduces the estimated oceanic LIP volumes by 50% to remove the amount that is associated with underplating. This results in a better comparison with continental LIPs where the component of underplating is typically not possible to estimate. The version #2 estimate of LIP volumes consists of the maximum LIP volumes including the underplate component for oceanic LIPs. Both LIP volume datasets are restricted to the last 260 Ma due to the availability of reliable volume data.

Each dataset has been Gaussian filtered to equidistant 1 Ma-intervals considering a minimum 2% stratigraphic uncertainty (95% confidence interval of normal distribution). The Gaussian filtering algorithm used is in detail described in Prokoph et al. (2004a). The mean sample age uncertainty is set larger for poorly stratigraphic constraint samples. The Gaussian filtered records for LIP occurrences and volumes are shown in Fig. 1.

3. Data analysis methods

Continuous wavelet transform (CWT) is applied to delineate temporal variations of cycle amplitudes and phase over a 20–500 Ma spectrum for all datasets, whereas cross-wavelet transform (XWT) is used to extract the cross-amplitude and instantaneous time lag (i.e. phase shift) between LIP and other geological records.

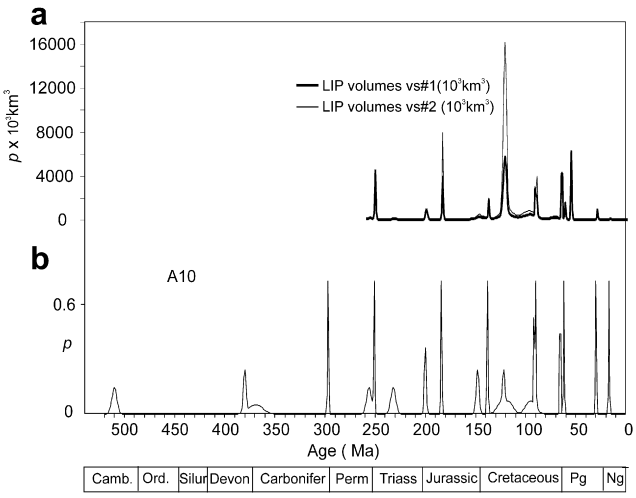

Figure 1. Gaussian filtered LIP volumes for last 260 Ma and A10 occurrences for last 520 Ma. For raw data see Ernst and Buchan (2001) and Table 1, for Gaussian filtered data see Table 2.

Wavelet analysis first emerged as a filtering and data compression method in the 1980s (e.g., Morlet et al., 1982). Wavelet analysis transforms a time-series into a frequency domain; it simultaneously transforms the 'depth' or 'time' domain and the 'scale' or 'frequency' domain by using various shapes and sizes of short filtering functions called wavelets. CWT allows for the

Table 1
LIP volumes.

Age (Ma)	1σ	Rating	Vol-vs.#1 (10^3 km^3)	Vol-vs.#2 (10^3 km^3)	Type	Event ID	Event name
17	0.5	A	175	175	Continental	1	Columbia
30	0.5	A	1200*	1200*	Continental	2	Afar
48	5	B	50$	100$	Oceanic	–	Metchosin (="Coast Range Basalt Province")
56*	0.5	A	7900*	7900*	Continental	5	NAVP
62	0.5	A	2000*	2000*	Continental	5	NAVP
65.5	0.5	A	8600	8600	Continental	6	Deccan
70	1	B	100$	200$	Oceanic	9	Carmacks
73	5	B	600	1200	Oceanic	7	Maud
73	5	B	1250	2500	Oceanic	8	Sierra
90	0.5	A	2250	4500	Oceanic	11	CCCIP
91.6	0.5	A	4400	4400	Continental	10	Madagascar
95	5	A	2000$	2000$	Continental	12	Alpha
96	5	B	750	1500	Oceanic	13	Wallaby
99	7.5	B	4550	9100	Oceanic	14	Hess
101	5	B	600	1200	Oceanic	15	Naturaliste
111	5	B	450	900	Oceanic	19	Nauru
118	5	A	3000*	6000*	Oceanic	18	Kerguelen
122	1.5	A	20,000#	57,000#	Oceanic	20	Ontong
123	5	A	4400	8800	Oceanic	21	Manihiki
123	6.5	B	50$	100$	Oceanic	22	Piñón
136	5	B	800	800	Continental	25	Gascoyne
138	0.5	A	2300	2300	Continental	24	Paraná–Etendeka
145	5	B	900	1800	Oceanic	26	Magellan
147	5	B	1250	2500	Oceanic	27	Shatsky
148	1.5	A	300	600	Oceanic	28	Sorachi
155	5	B	300$	300$	Continental	29	Argo
184	0.5	A	5000#	10,000#	Continental	31	Karoo–Ferrar
200	1	A	2500	2500	Continental	32	CAMP
214	7	B	225$	450$	Oceanic	33	Angayucham (=Ramparts Group volcanics)
232	2.5	A	500	1000	Oceanic	34	Wrangelia
251	0.5	A	5700	5700	Continental	36	Siberian
256	2.5	A	1000	1000	Continental	37	Emeishan

Estimation by Ernst and Buchan (2001) except for * Courtillot and Renne (2003), $ estimates from areal extend, # volume estimates from 5000 to 10,000 × 10^3 km^3.

Table 2
Gaussian filtered data.

Age (Ma)	A10 *p*	$^{87}Sr/^{86}Sr$	$\delta^{34}S$	LIP volumes vs#1(10^3 km^3)	LIP volumes vs#2(10^3 km^3)	Marine genera*	Age (Ma)	A10 *p*	$^{87}Sr/^{86}Sr$	$\delta^{34}S$	LIP volumes vs#1(10^3 km^3)	LIP volumes vs#2(10^3 km^3)	Marine genera*
Part-1													
0	0	0.709167	21.1264	0.0	0.0	189.7	71	0	0.707713	19.2839	160.7	321.4	84.3
1	0	0.709134	21.8869	0.0	0.0	227.3	72	0	0.707693	19.2951	150.5	300.9	105.2
2	0	0.70908	22.0149	0.0	0.0	161.1	73	0	0.707696	19.2447	148.7	297.3	125.8
3	0	0.709055	21.5815	0.0	0.0	198.2	74	0.00001	0.707624	19.1532	145.7	291.3	146.3
4	0	0.709042	21.596	0.0	0.0	114	75	0.00003	0.707618	19.044	137.8	275.5	166.5
5	0	0.709001	21.9447	0.0	0.0	150.5	76	0.00006	0.707584	19.0431	125.6	251.1	186.5
6	0	0.708958	21.9649	0.0	0.0	–13.7	77	0.00012	0.707518	19.0583	110.8	221.3	206.4
7	0	0.708949	22.32	0.0	0.0	22.3	78	0.00025	0.70746	18.9057	94.9	189.3	110
8	0	0.708937	22.0065	0.0	0.0	20	79	0.00048	0.707662	18.9278	79.9	158.9	129.4
9	0	0.708952	22.0175	0.0	0.0	55.5	80	0.00089	0.707542	18.6342	67.3	132.9	148.7
10	0	0.708921	21.9316	0.0	0.0	90.7	81	0.00158	0.707497	18.2425	58.5	113.8	167.7
11	0	0.708902	22.2279	0.0	0.0	125.7	82	0.00272	0.707464	18.1086	54.4	103.4	186.6
12	0	0.708857	22.4396	0.0	0.0	183.4	83	0.00448	0.707483	18.3081	55.9	102.9	205.2
13	0	0.70882	22.0326	0.0	0.0	217.9	84	0.00709	0.707474	18.2123	63.6	113.0	49.2
14	0	0.708795	21.9688	0.0	0.0	252.1	85	0.0108	0.70746	17.2443	77.9	134.2	5.4
15	0.00027	0.708771	21.8751	0.0	0.0	286	86	0.01579	0.707379	18.1425	99.1	166.7	–46.5
16	0.10798	0.708743	22.09	18.9	18.9	91.7	87	0.02218	0.707357	18.2658	127.4	210.4	–28.7
17	0.79789	0.70865	21.9	139.6	139.6	125.1	88	0.02995	0.707341	18.1779	163.0	266.0	–60.5
18	0.10798	0.708533	21.8	18.9	18.9	158.3	89	0.10798	0.707317	18.2011	446.2	814.7	–43
19	0.00027	0.708458	21.56	0.0	0.0	191.3	90	0.79789	0.707292	18.3897	2064.7	4011.6	–47.7
20	0	0.708372	22.0059	0.0	0.0	223.9	91	0.38837	0.707318	18.6175	2247.7	2670.7	–30.6
21	0	0.708347	22	0.0	0.0	–1.6	92	0.57938	0.707399	18.8501	2892.8	3103.0	–61.7
22	0	0.708313	21.9001	0.0	0.0	30.6	93	0.07365	0.70738	18.9664	456.1	695.3	–44.9
23	0	0.708254	21.8988	0.0	0.0	62.5	94	0.07821	0.707408	19.0058	423.6	690.7	–11.6
24	0	0.708236	21.6795	0.0	0.0	–90.8	95	0.07979	0.707481	19.058	451.7	743.8	4.8
25	0	0.708167	21.7	0.0	0.0	–59.4	96	0.07821	0.707463	19.0421	469.1	781.8	–38.4
26	0	0.708113	21.7	0.0	0.0	–28.2	97	0.07365	0.707459	18.9066	475.0	802.8	–22.4
27	0	0.708073	21.3231	0.0	0.0	2.8	98	0.06664	0.707462	18.5743	469.7	806.1	–31.8
28	0.00027	0.708018	21.3187	0.3	0.3	33.5	99	0.05794	0.707438	17.7801	454.3	792.7	–16.2
29	0.10798	0.707986	21.3221	129.6	129.6	–122.1	100	0.04839	0.707453	17.1615	430.6	764.5	–67.5
30	0.79789	0.707974	21.4021	957.5	957.5	–91.8	101	0.03884	0.707439	16.744	401.0	724.4	–52.2
31	0.10798	0.707932	21.5722	129.6	129.6	–61.8	102	0.02995	0.707451	16.3886	368.0	676.0	–37.1
32	0.00027	0.707889	21.7698	0.3	0.4	–32.1	103	0.02218	0.707451	15.7108	333.7	623.1	–22.2
33	0	0.707855	21.6497	0.0	0.1	–2.6	104	0.01579	0.707445	15.6043	300.5	569.5	–97.8
34	0	0.707834	21.9439	0.1	0.2	124.7	105	0.0108	0.707432	15.3327	270.2	518.8	–83.2
35	0	0.707817	22.2687	0.1	0.3	153.7	106	0.00709	0.707434	15.0616	244.3	474.4	–68.9
36	0	0.707733	22.1497	0.2	0.4	182.5	107	0.00709	0.707415	14.8971	224.2	439.5	–54.7
37	0	0.707761	22.3	0.4	0.7	211	108	0.0108	0.707403	15.6472	211.1	416.7	–78
38	0	0.70775	22.5641	0.5	1.1	19.9	109	0.01579	0.707392	15.9739	205.8	408.4	–64.2
39	0	0.707782	22.4314	0.8	1.6	48	110	0.02218	0.707368	16.0672	209.1	416.4	–50.5
40	0	0.707782	22.1558	1.1	2.2	75.8	111	0.02995	0.707334	16.1565	221.4	441.8	–37
41	0	0.707696	22.389	1.5	3.0	–72.6	112	0.03884	0.707263	16.1406	242.6	484.8	–56.4
42	0	0.707781	22.4	1.9	3.9	–45.2	113	0.04839	0.707261	15.9708	272.3	544.3	–43.3
43	0	0.707794	22.4	2.4	4.8	–18	114	0.05794	0.70724	15.7347	309.1	618.0	–30.3
44	0	0.707839	22.4	2.9	5.8	8.9	115	0.06664	0.707234	15.1992	351.1	702.2	–17.4
45	0	0.707754	22.0003	3.3	6.7	35.6	116	0.07365	0.707265	14.9063	397.1	795.8	–4.8
46	0	0.707751	22	3.7	7.4	62.1	117	0.07821	0.707275	15.4022	459.5	936.4	7.7
47	0	0.707798	22	3.9	7.8	88.3	118	0.07979	0.70732	15.5516	630.0	1389.1	20
48	0	0.707769	21.9993	4.0	8.0	114.3	119	0.07821	0.70738	15.2505	1229.1	3070.0	8.7
49	0	0.707764	20.6902	3.9	7.8	–169.4	120	0.10934	0.707391	15.0415	2716.1	7290.6	20.7
50	0	0.707742	19.8639	3.7	7.4	–143.8	121	0.21297	0.707396	16.6952	4795.1	13209.9	32.6
51	0	0.707705	18.4802	3.3	6.7	–118.4	122	0.26596	0.707412	17.3857	5846.9	16213.8	44.2
52	0	0.707746	18.03	2.9	5.8	–93.3	123	0.21297	0.707408	17.0443	4764.3	13146.8	55.7
53	0	0.707759	17.9558	2.5	4.9	–68.4	124	0.10934	0.707349	17.2866	2656.2	7167.6	67.1
54	0	0.707753	17.7443	4.2	6.2	–43.7	125	0.07365	0.707343	17.0231	1143.7	2893.7	2.8
55	0	0.70776	17.739	854.8	856.5	–19.3	126	0.06664	0.70746	17.1023	524.0	1168.5	13.8
56	0	0.707753	17.3317	6304.9	6306.4	–516	127	0.05794	0.70748	18.6474	338.6	682.1	24.7
57	0	0.707748	17.7957	854.7	856.4	–492	128	0.04839	0.707482	17.895	267.7	519.1	4.4
58	0	0.707773	17.5923	4.3	6.5	–581.7	129	0.03884	0.70747	17.5778	218.9	414.0	15
59	0	0.707749	18.154	3.3	6.6	–558.1	130	0.02995	0.707464	16.9537	179.2	327.3	–14.1
60	0.00027	0.707807	18.1501	5.8	11.0	–534.8	131	0.02218	0.707473	17.0843	148.0	257.2	–3.8
61	0.10798	0.707814	18.15	224.4	232.8	–693.1	132	0.01579	0.707441	17.6692	125.3	204.3	6.27
62	0.79789	0.707775	18.7608	1609.0	1622.2	–670.2	133	0.0108	0.70742	16.38	110.4	167.6	16.22
63	0.10798	0.707821	18.9709	236.0	256.0	–728.9	134	0.00709	0.707406	16.3242	102.1	145.3	11.01
64	0.00886	0.707833	18.9803	106.0	135.2	–706.4	135	0.00448	0.707394	17.4607	98.9	135.2	20.66
65	0.48394	0.707862	18.9033	4203.0	4244.0	–684.1	136	0.00272	0.707385	17.4502	100.3	136.1	30.16
66	0.48394	0.707836	17.4117	4217.3	4272.8	–243.5	137	0.10798	0.707365	17.3745	351.9	392.8	24
67	0.00886	0.707791	18.8377	148.5	220.9	–221.6	138	0.79789	0.707349	18.257	1945.0	1995.9	33.2
68	0	0.707785	18.9015	95.0	190.0	–199.9	139	0.10798	0.707319	18.3654	366.8	431.7	9.75
69	0	0.707759	19.1312	131.5	262.9	51.5	140	0.00027	0.707259	15.4784	129.4	211.6	18.66
70	0	0.707727	19.2274	163.3	326.7	72.8	141	0.00012	0.707263	13.1158	140.5	241.8	–6.58

(*Continued on next page*)

Table 2 (*Continued*)

Age (Ma)	A10 *p*	$^{87}Sr/^{86}Sr$	$\delta^{34}S$	LIP volumes vs#1(10^3 km^3)	LIP volumes vs#2(10^3 km^3)	Marine genera*	Age (Ma)	A10 *p*	$^{87}Sr/^{86}Sr$	$\delta^{34}S$	LIP volumes vs#1(10^3 km^3)	LIP volumes vs#2(10^3 km^3)	Marine genera*
Part-2													
142	0.00009	0.707276	13.0023	152.7	273.5	2.03	212	0	0.707749	18.9209	12.3	24.6	−7.84
143	0.00103	0.707324	13.0001	164.5	303.6	−3.5	213	0	0.707734	18.9512	12.7	25.4	12.02
144	0.0076	0.707321	13	175.9	332.0	4.83	214	0	0.707715	18.9514	12.8	25.6	12.48
145	0.03599	0.707299	13	190.6	365.3	13.01	215	0	0.707704	18.8113	12.7	25.4	12.85
146	0.10934	0.707231	13.0001	214.3	415.3	124.06	216	0	0.707705	18.7543	12.3	24.6	13.14
147	0.21297	0.707188	13.0377	242.3	472.2	131.96	217	0	0.707703	18.8801	11.7	23.4	26.85
148	0.26596	0.707163	16.0002	250.1	487.6	139.72	218	0	0.707696	19.0565	10.9	21.8	26.98
149	0.21297	0.707109	16	221.9	430.0	161.85	219	0	0.707684	19.2308	9.9	19.9	27.04
150	0.10934	0.707024	16	175.4	335.1	169.33	220	0	0.707671	19.3747	8.9	17.8	27.01
151	0.03599	0.706985	16	136.3	254.4	189.68	221	0.00001	0.707666	19.4817	7.8	15.6	26.91
152	0.0076	0.706931	16	110.1	199.8	196.89	222	0.00005	0.707669	19.5474	6.7	13.4	26.74
153	0.00103	0.706874	16	91.1	159.9	203.97	223	0.00024	0.707653	18.046	5.7	11.5	19.49
154	0.00009	0.706854	16	75.2	126.9	218.41	224	0.00095	0.707624	17.9001	5.1	10.2	19.16
155	0	0.706847	16	61.4	98.9	225.22	225	0.00317	0.707606	17.8998	5.3	10.6	18.76
156	0	0.706865	15.9999	49.6	75.7	234.2	226	0.00896	0.707597	17.8986	7.4	14.9	18.29
157	0	0.706884	15.7084	39.6	57.2	240.74	227	0.0216	0.707601	17.8903	13.1	26.2	17.75
158	0	0.706886	15.4001	31.3	42.6	191.18	228	0.04437	0.707613	17.8373	23.9	47.8	−29.86
159	0	0.706874	15.4006	24.4	31.4	197.47	229	0.07767	0.707636	17.6277	40.1	80.3	−30.54
160	0	0.706855	15.4237	18.7	22.9	207.62	230	0.11588	0.707678	17.4056	58.9	117.8	−31.3
161	0	0.706851	15.8395	14.1	16.5	213.65	231	0.14731	0.707713	17.5076	74.3	148.7	−32.11
162	0	0.706856	16.156	10.3	11.6	186.88	232	0.15958	0.707725	18.2927	80.3	160.5	−33
163	0	0.706881	16.1469	7.4	8.1	184.31	233	0.14731	0.707726	19.2869	74.0	148.0	−119.95
164	0	0.707018	16.1415	5.1	5.5	187.63	234	0.11588	0.707723	20.5775	58.2	116.3	−120.97
165	0	0.70712	16.9574	3.4	3.6	184.15	235	0.07767	0.70772	23.026	39.0	78.0	−122.05
166	0	0.707106	18.6813	2.2	2.3	138.87	236	0.04437	0.707726	23.9151	22.3	44.6	−123.2
167	0	0.707084	20.1853	1.4	1.4	125.49	237	0.0216	0.707746	23.1014	10.9	21.7	−178.57
168	0	0.707092	18.9971	0.8	0.8	121.97	238	0.00896	0.707778	22.409	4.5	9.0	−179.84
169	0	0.707146	17.2493	0.5	0.5	126.99	239	0.00317	0.707833	22.8929	1.6	3.2	−181.17
170	0	0.707241	16.4589	0.3	0.3	70.4	240	0.00095	0.707869	23.2407	0.5	1.0	−232.22
171	0	0.707282	17.0917	0.1	0.1	75.19	241	0.00024	0.707878	22.6934	0.1	0.3	−233.67
172	0	0.707292	17.7408	0.1	0.1	12.36	242	0.00005	0.707891	21.7016	0.0	0.1	−235.18
173	0	0.707295	17.9352	0.0	0.0	16.91	243	0.00001	0.707943	22.8395	0.0	0.0	−291.42
174	0	0.707291	17.9011	0.0	0.0	21.34	244	0	0.708054	25.9221	0.0	0.0	−293.04
175	0	0.70729	17.9	0.0	0.0	25.66	245	0.00001	0.708131	26.3229	0.0	0.0	−342.72
176	0	0.707291	17.9009	0.0	0.0	−36.14	246	0.00005	0.708152	26.327	0.1	0.1	−344.45
177	0	0.707299	18.0826	0.0	0.0	−32.05	247	0.00024	0.708123	25.7205	0.2	0.2	−346.24
178	0	0.707306	22.7007	0.0	0.0	−28.08	248	0.00095	0.707986	19.6957	1.0	1.0	−393.58
179	0	0.707292	23.1057	0.0	0.0	−24.22	249	0.00317	0.707794	16.6393	4.7	4.7	−395.48
180	0	0.707248	22.5517	0.0	0.0	−8.97	250	0.10798	0.70764	17.1165	624.5	624.5	−425.42
181	0	0.707193	21.1139	0.0	0.0	−5.33	251	0.79789	0.707513	17.7684	4569.5	4569.5	−212.41
182	0.00027	0.707147	18.7136	1.3	2.7	−1.81	252	0.10798	0.707406	18.3852	659.9	659.9	−214.46
183	0.10798	0.707116	17.4601	539.9	1079.8	2.11	253	0.07767	0.707327	18.9415	79.2	79.2	−216.55
184	0.79789	0.707134	17.1609	3989.4	7978.9	5.42	254	0.11588	0.707301	19.4297	115.9	115.9	−66.2
185	0.10798	0.70719	15.7734	539.9	1079.8	8.62	255	0.14731	0.707305	19.8524	147.3	147.3	−68.38
186	0.00027	0.70723	14.4379	1.3	2.7	11.71	256	0.15958	0.707288	20.217	159.6	159.6	−70.62
187	0	0.707261	14.3132	0.0	0.0	−18.8	257	0.14731	0.707208	19.6539	147.3	147.3	−72.9
188	0	0.707298	14.6137	0.0	0.0	−15.92	258	0.11588	0.707123	11.0246	115.9	115.9	−75.22
189	0	0.707345	15.3098	0.0	0.0	−13.14	259	0.07767	0.707096	11.0001	77.7	77.7	−77.59
190	0	0.707398	15.1189	0.0	0.1	−63.46	260	0.04437	0.707128	11.0006	44.4	44.4	−80.01
191	0	0.707443	14.8533	0.1	0.1	−60.89	261	0.0216	0.707196	11.0043			178.04
192	0	0.707482	14.6072	0.1	0.2	−58.42	262	0.00896	0.707197	11.0298			175.55
193	0	0.707528	14.4269	0.1	0.3	−56.05	263	0.00317	0.707096	11.1977			173.01
194	0	0.707583	14.3169	0.2	0.4	−121.28	264	0.00095	0.707067	12.0092			170.44
195	0	0.707652	14.7292	0.3	0.6	−119.11	265	0.00024	0.707119	13.4035			167.82
196	0.00013	0.707717	24.1911	0.8	1.3	−117.03	266	0.00005	0.707184	13.9802			260.67
197	0.00443	0.707748	24.0619	11.8	12.4	−170.56	267	0.00001	0.707188	14.0819			257.99
198	0.05399	0.707757	23.5983	135.9	136.9	−168.68	268	0	0.70714	14.0837			255.26
199	0.24197	0.707759	22.3601	606.2	607.5	−209.39	269	0	0.707102	13.9591			252.51
200	0.39894	0.707745	19.7228	999.1	1000.8	−103.71	270	0	0.707085	13.6231			249.71
201	0.24197	0.707734	16.1006	607.2	609.5	−102.11	271	0	0.707067	13.5371			280.22
202	0.05399	0.707749	13.5559	137.9	140.9	−100.61	272	0	0.707037	13.7333			277.36
203	0.00443	0.707821	15.7744	14.8	18.5	−99.2	273	0	0.707011	14.5791			274.47
204	0.00013	0.70799	17.9649	5.0	9.6	−37.55	274	0	0.706997	15.1666			271.55
205	0	0.708046	18.0653	5.6	11.2	−36.32	275	0	0.707006	15.1211			268.6
206	0	0.708043	18.1393	6.7	13.3	−35.18	276	0	0.70706	14.4292			229.29
207	0	0.708044	18.1913	7.8	15.6	−34.13	277	0	0.707114	13.1536			226.29
208	0	0.708042	17.8911	8.9	17.8	−10.83	278	0	0.707133	12.4719			223.25
209	0	0.708032	17.5372	9.9	19.9	−9.95	279	0	0.707131	12.1986			220.19
210	0	0.707971	17.7571	10.9	21.8	−9.17	280	0	0.707127	12.2137			187.77
211	0	0.707782	18.7694	11.7	23.4	−8.46	281	0	0.707131	12.5251			184.66

Table 2 (*Continued*)

Age (Ma)	A10 *p*	$^{87}Sr/^{86}Sr$	$\delta^{34}S$	LIP volumes vs#1(10^3 km^3)	LIP volumes vs#2(10^3 km^3)	Marine genera*	Age (Ma)	A10 *p*	$^{87}Sr/^{86}Sr$	$\delta^{34}S$	LIP volumes vs#1(10^3 km^3)	LIP volumes vs#2(10^3 km^3)	Marine genera*
Part-3													
282	0	0.707164	12.9692			181.53	353	0.00418	0.708139	21.1019			−146.16
283	0	0.707227	13.2844			178.37	354	0.00574	0.708181	20.4954			−148.73
284	0	0.707288	13.4259			175.19	355	0.00771	0.70823	19.8873			−151.26
285	0	0.707341	13.4763			181.32	356	0.01016	0.708284	19.7276			−153.76
286	0	0.707397	13.4927			178.1	357	0.01311	0.708329	19.7037			−156.21
287	0	0.707476	13.4978			174.86	358	0.01658	0.708358	19.7005			−158.62
288	0	0.707584	13.4989			171.6	359	0.02054	0.708379	19.7001			−160.99
289	0	0.707684	13.1005			168.32	360	0.02494	0.708398	19.7			−248.48
290	0	0.707735	12.6006			113.53	361	0.02966	0.708414	19.7			−250.76
291	0	0.707744	12.5999			110.22	362	0.03457	0.708425	19.7			−252.99
292	0	0.707743	12.5998			106.89	363	0.03947	0.708433	19.7			−255.18
293	0	0.70778	12.5994			103.56	364	0.04416	0.708432	19.7			−257.32
294	0	0.707866	12.5981			100.2	365	0.04841	0.708419	19.7012			−300.07
295	0.00027	0.70793	12.5937			55.34	366	0.05199	0.708397	20.0302			−302.11
296	0.10798	0.70796	12.5809			51.96	367	0.05471	0.708363	23.1873			−304.1
297	0.79789	0.707979	12.554			15.57	368	0.05641	0.708298	23.2996			−306.05
298	0.10798	0.708005	12.5242			12.18	369	0.05699	0.708214	23.3			−307.94
299	0.00027	0.708044	12.5064			59.77	370	0.05641	0.708163	23.3			−332.45
300	0	0.708093	12.4855			56.36	371	0.05471	0.708143	23.3			−334.23
301	0	0.708143	12.3462			52.93	372	0.05199	0.708133	23.3001			−335.96
302	0	0.708185	11.8957			49.51	373	0.04841	0.708126	23.3002			−337.64
303	0	0.708214	11.6556			46.07	374	0.04416	0.708121	23.301			−339.26
304	0	0.708236	11.6151			55.13	375	0.03947	0.70812	23.3041			−228.49
305	0	0.708256	11.7365			51.69	376	0.03457	0.708119	23.3171			−230
306	0	0.708269	12.2758			48.24	377	0.03599	0.708118	23.3709			−231.45
307	0	0.708275	13.0445			76.8	378	0.10934	0.708116	23.5826			−232.84
308	0	0.708277	13.4045			73.35	379	0.21297	0.708111	24.2604			−168.82
309	0	0.70828	13.5153			69.9	380	0.26596	0.708104	25.4971			−170.13
310	0	0.708286	13.6467			34.95	381	0.21297	0.70809	26.4337			−171.33
311	0	0.70829	13.9179			31.5	382	0.10934	0.708063	26.7465			−124.1
312	0	0.708293	14.3193			−15.45	383	0.03599	0.708018	26.6512			−125.2
313	0	0.708294	14.7533			−18.89	384	0.0076	0.707967	25.8671			−126.2
314	0	0.708291	15.1201			−22.33	385	0.00418	0.707924	24.4323			−127.2
315	0	0.708283	15.4076			−55.26	386	0.00299	0.70789	23.6851			23
316	0	0.70827	15.5981			−58.69	387	0.00209	0.707866	23.4217			22.1
317	0	0.708254	15.6284			−62.11	388	0.00143	0.707854	23.1413			21.4
318	0	0.708233	15.4501			−65.52	389	0.00096	0.707851	22.6252			99.7
319	0	0.708199	15.1444			−75.43	390	0.00063	0.707852	21.7722			99.1
320	0	0.70816	14.9464			−78.83	391	0.00041	0.707857	20.635			98.6
321	0	0.708123	14.9688			−82.21	392	0.00026	0.707865	19.4038			183.1
322	0	0.708073	15.0476			−85.59	393	0.00016	0.707877	18.2868			182.7
323	0	0.708017	14.9391			91.54	394	0.0001	0.70789	17.4198			182.4
324	0	0.70799	14.6096			88.19	395	0.00006	0.707899	16.9035			207.6
325	0	0.707987	14.3027			84.85	396	0.00003	0.707902	16.7243			207.5
326	0	0.707983	14.1447			81.53	397	0.00002	0.707903	16.6601			207.4
327	0	0.707966	14.0711			173.72	398	0.00001	0.707904	16.5652			235.9
328	0	0.707931	13.9941			170.43	399	0.00001	0.707908	16.3615			235.9
329	0	0.707879	13.9055			167.15	400	0	0.707918	15.9566			236
330	0	0.707823	13.8686			163.89	401	0	0.707938	15.3278			236.3
331	0	0.707778	13.9615			160.65	402	0	0.707978	14.6856			236.6
332	0	0.707752	14.1426			157.43	403	0	0.708041	14.499			196.4
333	0	0.707744	14.2528			154.23	404	0	0.708118	15.3917			196.9
334	0	0.70775	14.2966			151.05	405	0	0.708194	17.6014			197.4
335	0	0.707763	14.372			147.9	406	0	0.708264	20.1276			198
336	0	0.707776	14.7041			105.26	407	0	0.708335	21.8059			66.8
337	0	0.707789	15.4753			102.15	408	0	0.708422	22.6032			67.5
338	0	0.707806	16.417			99.07	409	0	0.708523	22.9363			68.4
339	0.00001	0.707823	17.2977			96.01	410	0	0.70861	23.131			0.4
340	0.00001	0.707825	18.0314			92.98	411	0	0.708664	23.3554			1.4
341	0.00002	0.707812	18.5444			89.97	412	0	0.708693	23.5898			−41.9
342	0.00003	0.707803	18.5993			86.99	413	0	0.708706	23.8394			−40.7
343	0.00006	0.707812	18.0895			84.04	414	0	0.708712	24.1251			−82.9
344	0.0001	0.707833	17.7435			81.13	415	0	0.708714	24.4705			−81.44
345	0.00016	0.707852	17.6722			78.24	416	0	0.708715	24.9078			−48.44
346	0.00026	0.707865	17.7124			3.88	417	0	0.708712	25.4545			−46.84
347	0.00041	0.70788	17.9184			1.06	418	0	0.708704	26.0631			−45.15
348	0.00063	0.707903	18.6073			−1.73	419	0	0.708689	26.6049			32.64
349	0.00096	0.70794	19.8799			−4.49	420	0	0.708666	26.95			34.52
350	0.00143	0.707991	20.8329			−7.21	421	0	0.708633	27.0916			36.5
351	0.00209	0.708048	21.1757			−9.9	422	0	0.708589	27.1488			105.58
352	0.00299	0.708098	21.2424			−12.55	423	0	0.708535	27.2236			122.26

(*Continued on next page*)

Table 2 (*Continued*)

Age (Ma)	A10 *p*	$^{87}Sr/^{86}Sr$	$\delta^{34}S$	LIP volumes vs#1(10^3 km^3)	LIP volumes vs#2(10^3 km^3)	Marine genera*	Age (Ma)	A10 *p*	$^{87}Sr/^{86}Sr$	$\delta^{34}S$	LIP volumes vs#1(10^3 km^3)	LIP volumes vs#2(10^3 km^3)	Marine genera*
Part-4													
424	0	0.708481	27.3177			124.53	495	0	0.709111	32.1415			–337.36
425	0	0.708436	27.3606			126.91	496	0	0.709105	32.1143			–325.68
426	0	0.708405	27.2495			129.38	497	0	0.70909	32.8351			–320.33
427	0	0.708382	26.9048			71.96	498	0	0.709076	34.12			–308.32
428	0	0.708364	26.3579			74.64	499	0.00001	0.709074	35.5277			–283.65
429	0	0.708345	25.7988			–44.08	500	0.00005	0.709077	36.7752			–271.31
430	0	0.708319	25.5608			–41.19	501	0.00024	0.709081	37.7295			–226.14
431	0	0.708284	26.087			–38.2	502	0.00095	0.709082	38.3279			–213.47
432	0	0.708242	27.352			–35.1	503	0.00317	0.709083	38.5603			–213.97
433	0	0.708204	28.424			–31.9	504	0.00896	0.709083	38.4691			–183.29
434	0	0.708175	28.9556			–28.58	505	0.0216	0.709084	38.1337			–144.12
435	0	0.708152	29.2316			–25.16	506	0.04437	0.709138	37.6428			–130.77
436	0	0.708129	29.4605			–146.3	507	0.07767	0.70916	37.0693			–128.75
437	0	0.708107	29.7066			–142.66	508	0.11588	0.708943	36.4611			–115.07
438	0	0.708084	29.927			–138.9	509	0.14731	0.708804	35.8458			–103.71
439	0	0.708057	29.9406			–209.7	510	0.15958	0.70879	35.2407			–89.67
440	0	0.70802	29.4217			–205.72	511	0.14731	0.708774	34.6588			–75.46
441	0	0.707986	28.1398			–201.63	512	0.11588	0.708758	34.1107			–61.08
442	0	0.707968	26.3328			–197.42	513	0.07767	0.708739	33.6037			–40.02
443	0	0.707961	24.5483			–193.1	514	0.04437	0.70872	33.1456			–25.28
444	0	0.707956	23.1576			–67.66	515	0.0216	0.708703	32.7975			–10.37
445	0	0.707949	22.2675			–63.11	516	0.00896	0.708687	32.9023			2.23
446	0	0.70794	21.8754			264.59	517	0.00317	0.708673	33.376			17.5
447	0	0.707927	21.9731			269.39	518	0.00095	0.708658	33.5513			32.95
448	0	0.707914	22.4921			301.3	519	0.00024	0.708639	33.6085			173.09
449	0	0.707905	23.1411			351.63	520	0.00005	0.708618	33.6601			188.91
450	0	0.707904	23.6991			356.79							
451	0	0.70791	24.2087			362.07							
452	0	0.707926	24.7292			367.47							
453	0	0.707955	25.245			408.29							
454	0	0.707993	25.6599			413.94							
455	0	0.708029	25.8326			419.72							
456	0	0.708057	25.717			425.62							
457	0	0.70808	25.4217			398.05							
458	0	0.708102	25.0586			404.21							
459	0	0.708129	24.6539			410.5							
460	0	0.708166	24.1585			416.91							
461	0	0.708221	23.4239			229.76							
462	0	0.708295	22.332			236.45							
463	0	0.708374	21.4508			121.76							
464	0	0.708447	21.5106			14.71							
465	0	0.708522	22.287			21.79							
466	0	0.708612	23.4152			29.01							
467	0	0.708711	24.6849			36.36							
468	0	0.708795	25.8873			–8.15							
469	0	0.708843	26.8031			–0.52							
470	0	0.708858	27.3191			7.25							
471	0	0.708858	27.5025			15.16							
472	0	0.708859	27.5302			–62.29							
473	0	0.708865	27.5885			–54.1							
474	0	0.708877	27.8328			–45.77							
475	0	0.708896	28.3201			–37.29							
476	0	0.708919	28.9359			–267.67							
477	0	0.708939	29.5101			–258.91							
478	0	0.70895	29.9636			–249.99							
479	0	0.708951	30.2883			–361.94							
480	0	0.70895	30.4858			–352.73							
481	0	0.708956	30.5304			–343.38							
482	0	0.708972	30.3244			–333.88							
483	0	0.708994	29.7264			–324.22							
484	0	0.709013	28.9989			–367.92							
485	0	0.709029	28.8066			–357.96							
486	0	0.709041	29.1662			–347.85							
487	0	0.709051	29.7916			–337.59							
488	0	0.709061	30.5368			–327.17							
489	0	0.70907	31.3242			–361.6							
490	0	0.709079	32.0648			–350.87							
491	0	0.709087	32.6415			–353.99							
492	0	0.709095	32.9378			–342.95							
493	0	0.709102	32.8921			–346.24							
494	0	0.709109	32.5515			–334.88							

automatic localization of periodic signals, gradual shifts and abrupt interruptions, trends and onsets of trends in time-series (Rioul and Vetterli, 1991). The wavelet coefficients W of a time-series $x(s)$ are calculated by a simple convolution

$$W_\psi(a,b) = \left(\frac{1}{\sqrt{a}}\right)\int x(s)\psi\left(\frac{s-b}{a}\right)\mathrm{d}s \quad (1)$$

where ψ is the mother wavelet, a is the scale factor that determines the characteristic frequency or wavelength, and b represents the shift of the wavelet over $x(s)$ (Prokoph and Barthelmes, 1996).

The bandwidth resolution for a wavelet transform varies with

$$\Delta a = \frac{\sqrt{2}}{4\pi a l} \quad (2)$$

and a location resolution

$$\Delta b = \frac{a l}{\sqrt{2}} \quad (3)$$

Due to Heisenberg's uncertainty principle $\Delta a \Delta b \geq 1/4\pi$, the resolution of Δb and Δa cannot be arbitrarily small (e.g., Prokoph and Barthelmes, 1996). The parameter l is used to modify the

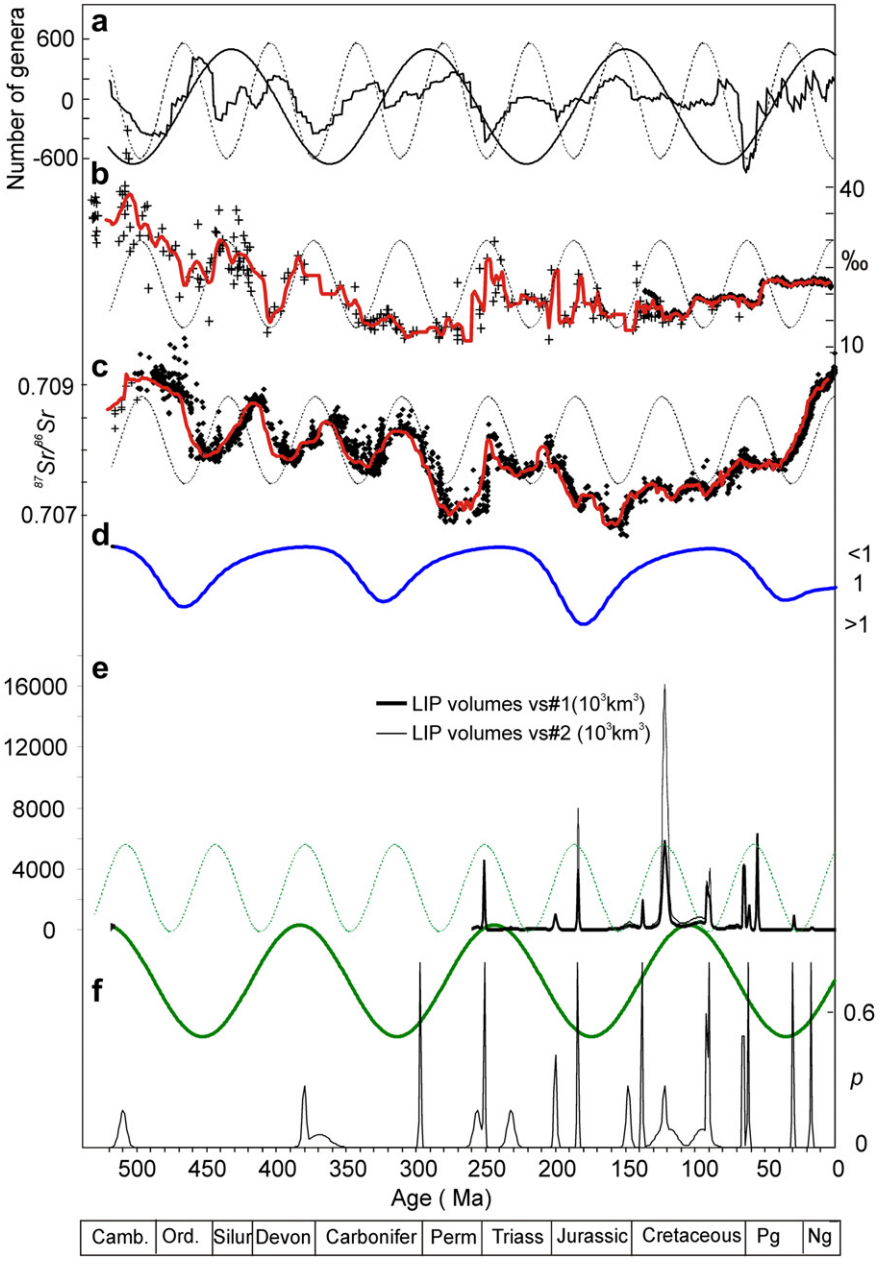

Figure 2. Geological records of last 520 Ma with best-fit 140–170 Ma and 65 Ma sine waves. a: Third order-polygonal detrended well-dated marine genera (Rhode and Muller, 2005); b: diamonds: $\delta^{34}S_{barite}$ (Paytan et al., 2004), crosses: $\delta^{34}S$ of structurally substituted sulfate (SSS) (Kampschulte and Strauss, 2004), red line: Gaussian filtered time-series; c: $^{87}Sr/^{86}Sr$ data: diamonds: low-Mg fossil shell data (Prokoph et al., 2008), crosses: whole rock samples (Shields and Veizer, 2002); d: simplified cosmic ray flux (CRF) ratio model (Shaviv and Veizer, 2003); e: LIP's volume (Ernst and Buchan, 2001; Berner, 2002) × probability of occurrence (Prokoph et al., 2004a), note: as the total probability for each event equals 1, the total sum of $p \times$ volumes = sum all volumes; f: probability (of occurrence) of Gaussian filtered precisely dated (1‰ < 2.5 Ma) LIP's, mostly flood and oceanic plateau basalts (Prokoph et al., 2004b), bottom: time scale (Gradstein et al., 2005).

bandwidth resolution either in favor of time or in favor of frequency. In this study, the CWT was used with the Morlet wavelet as the mother function (Morlet et al., 1982), which is expressed in its shifted and scaled version as

$$\psi^{l}_{a,b}(s) = \sqrt[4]{\pi}\sqrt{al}\, e^{-\frac{i2\pi(s-b)}{a}}\, e^{-\frac{1}{2}\left(\frac{s-b}{al}\right)^2} \quad (4)$$

The Morlet wavelet is a sinusoid with wavelength/scale a modulated by a Gaussian function (Torrence and Compo, 1998). Edge effects of the wavelet coefficients occur at the beginning and end of the analyzed time-series and increase with increasing wavelength (scale) and parameter l forming a 'cone of influence of edge effects' (Torrence and Compo, 1998). The cones of >10% influences of the edge effects are based on the wavelet-analysis parameters used and are illustrated in the scalograms. The amplitude-reducing feature of edge effects has been reduced by dividing the uncorrected amplitudes by a wavelet coefficients of control sine waves of 32 Ma, 65 Ma, and 140 Ma wavelengths for the respective wavebands.

The wavelet coefficients W are normalized by using the L1 normalization ($1/a$), replacing the commonly used $1/\sqrt{a}$, L2, or L^2 normalization (see Eq. (1)), which allow for an interpretation of wavelet coefficients in terms of Fourier amplitudes (e.g., Prokoph and Barthelmes, 1996). In addition, the L2 normalization of the Morlet wavelet commonly leads to overvaluing wavelet coefficients in long wavelengths compared to shorter ones, as discussed in detail by Schaefli et al. (2007). The parameter $l = 10$ was chosen for all analyses, which provides sufficiently precise results in the resolution of time and scale (e.g., Prokoph et al., 2004b). The series of wavelengths $a_{W\max}(b)$ with the strongest local wavelet coefficient $W(a, b)$ were extracted from the wavelet-coefficient matrix for waveband of 28–35 Ma, 60–70 Ma, and 130–150 Ma, because these series determine the strongest amplitude and their related wavelength in their respective waveband, independent of their absolute amplitude compared to the rest of the analyzed time-series. The wavelet-analysis technique used in this article is explained in detail in Prokoph and Barthelmes (1996). The matrix of the wavelet coefficients $W_l(a, b)$, the so-called 'scalogram', was coded in color scale (orange highest, blue lowest $W_l(a, b)$) for better graphical interpretation.

The cross-wavelet spectrum of two series $x(t)$ and $y(t)$ is defined by

$$W_{xy}(a,b) = W_x(a,b)W^{*}_{y}(a,b) \quad (5)$$

where $W_x(a, b)$ and $W_y(a, b)$ are the continuous wavelet transform of $x(t)$ and $y(t)$ respectively, and * denotes the complex conjugate (e.g., Jury et al., 2002; Grinsted et al., 2004; Labat, 2005). The phase difference is defined by

$$\Delta\phi(b) = \tan^{-1}\frac{\int_{a_1}^{a_2} \mathrm{Im}(W_{xy}(a,b))\,da}{\int_{a_1}^{a_2} \mathrm{Re}(W_{xy}(a,b))\,da} \quad (6)$$

with b corresponding to the time lag b (Jury et al., 2002). "Im" and "Re" indicate the imaginary and real parts, respectively. The mother wavelet and parameters used in this study are the same as for the wavelet-analysis description provided above. For a detailed explanation of advantages and disadvantages of the normalization types regarding accuracy of the energy spectrum, amplitudes and white noise, as well as variance and bias of arbitrary estimated cross-wavelet spectra depending on the algorithms applied one can refer to Maraun and Kurths (2004) and Maraun et al. (2007).

4. Results

The A10-LIP occurrence record consists of over 20 discrete events with decreasing frequency toward older age (Fig. 1b). In contrast, the LIP volumes for the last 260 Ma are dominated by four roughly equally ~65 Ma spaced large volume events, independently if version 31 or #2 are considered (Fig. 1a, Tables 1 and 2). Such an ~60–65 Ma stationary cycle with minor (±5 Ma) temporal fluctuations can be fitted to all geochemical and the detrended marine genera records (Fig. 2). In addition, a ~140 Ma cycle can be fitted to A10-LIP and marine genera record that is approximately inverse to the cosmic ray flux cycle promoted as major climate driver by Shaviv and Veizer (2003). Spectral analysis shows that all records exhibit considerable noise, but similar spectral peaks at ~140 Ma and 60–65 Ma. An ~28–35 Ma broadband spectral excursion is significant in the LIP volume data of the last 260 Ma (Fig. 3). The LIP volume record don't exhibit ~140 Ma cyclicity, but ~170 Ma cyclicity, which are essentially the same as within the uncertainties caused by the limited record length and hence limited low-frequency resolution.

Wavelet analysis highlights striking similarities in the cycle pattern between marine genera and LIP records during the last ~350 Ma, with an abrupt onset of a ~32 Ma cyclicity at ~135 Ma (Fig. 4a, b, e, f). Wavelet analysis extracted major 60–68 Ma and 140–160 Ma wavelengths for all geological records that slightly fluctuate in time (Fig. 4). Fossil and isotope record show all an increasing magnitude of the ~62 Ma cyclicity for Cambrian to Carboniferous, that is not evident in the LIP record. On average the dominant LIP cycle in the 60–80 Ma waveband is 64.5 Ma, slightly longer than the ~62 Ma cycle in fossil and geochemical records. In addition there is a ~100 Ma cyclicity for $^{87}Sr/^{86}Sr$, and for the last ~135 Ma, a ~28–35 Ma cycle for LIP probability (A10), LIP volume and marine biodiversity. The CWT parameters used implement a bandwidth uncertainty of ~±3% (see Eq. (2)). The temporal resolution is weaker (see Eq. (3)). For example a ~62 (60–65) Ma cycle detected at 300 Ma represents (to a 95% confidence level) an average wavelength for the interval of 300 ± 210 Ma (i.e. 90–510 Ma), and (to a 66% confidence level) an average for 300 ± 105 Ma.

In average, the wavelet coefficient representing cycle amplitude is significantly different for the ~32, ~62 and ~140 Ma wavelengths, except for marine genera that have about the same magnitude for all cycle lengths (Table 3). Thus, most high spectral values (Fig. 2) can be attributed to short-term fluctuations at

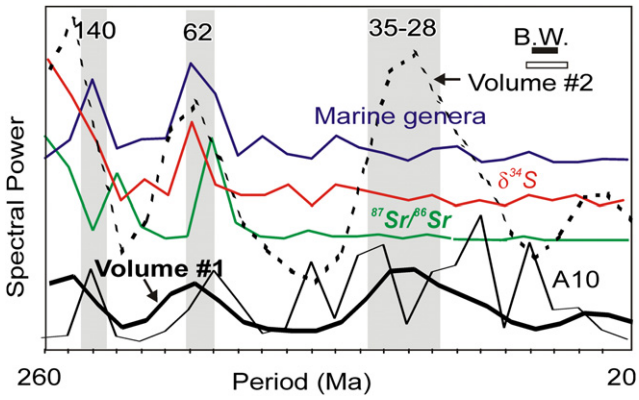

Figure 3. Spectral analysis. Spectral Power estimates for the linear detrended geological records (Fig. 2) for the last 520 Ma: vertical gray bars: bandwidth of proposed 140 Ma, ~62 Ma, and 35–28 Ma cycles, B.W. bandwidth uncertainty, note: the bandwidth for LIP volume is wider because of the shorter dataset (0–260 Ma). Lowest value for each record equals zero variance.

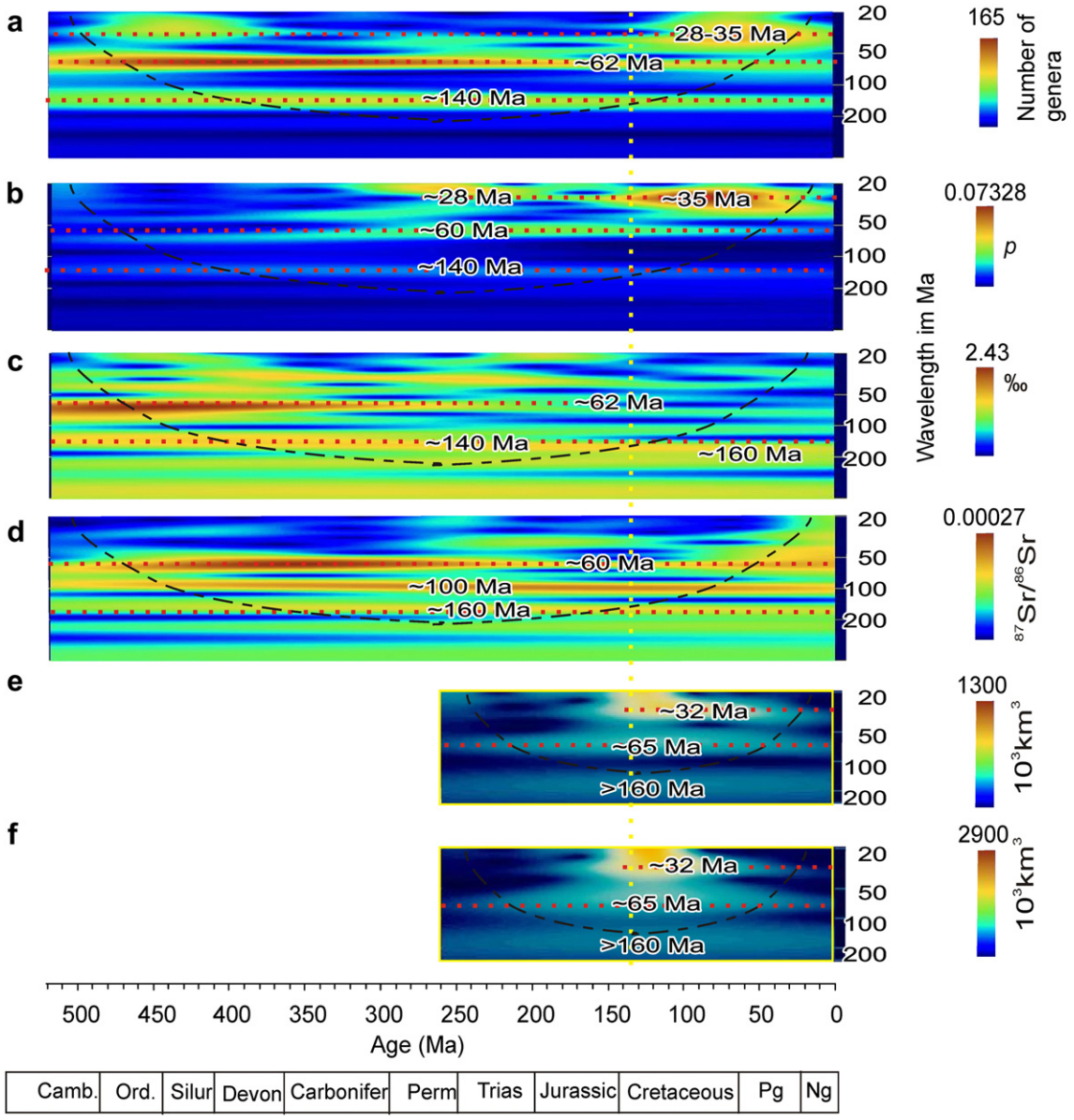

Figure 4. Wavelet analysis. a: Wavelet scalogram of detrended marine genera record; b: wavelet scalogram of marine biodiversity record; c: wavelet scalogram of probability of LIP occurrence (A10 dataset); d: wavelet scalogram of sulfur isotopes of sulfate; e: wavelet scalogram of $^{87}Sr/^{86}Sr$ record; f: LIP volumes, version #1 for last 260 Ma. Bottom: time scale (Gradstein et al., 2005). Stripped curve separates frequency–time space of edge effect of <20% (above line) from >20% (below line), red dotted lines mark cycle bands, color code for wavelet amplitudes on right, vertical yellow dotted line marks the onset of ~32 Ma cyclicity in LIP and fossil records at ~135 Ma.

different wavelengths (i.e. noise), with only ~140 Ma, 62–65 Ma, and 28–35 Ma cycle bands reoccurring with at least four consecutive repetitions (Fig. 4). With the mother wavelet used and parameter $l = 10$, jumps and gradual changes in the temporal pattern can only be detected in relatively short wavelengths (e.g., to 66% ±50 Ma for a ~28 Ma-cycle). Thus, the change in the pattern at ~135 Ma has a temporal uncertainty of ~±50 Ma at a 66% confidence level.

Table 3
Cycle amplitudes.

Cycle length	32 Ma	65 Ma	140 Ma
Interval	0–135 Ma	135–260 Ma	0–260 Ma
LIP vol v#1	498	316	276
LIP vol v#2	931	666	584
$\delta^{34}S$	0.79	0.66	1.78
Marine genera	124	127	123

Before ~135 Ma, the ~65 Ma and 140 Ma LIP cyclicities are followed by a ~20 Ma delayed increase in the incorporation of heavy sulfur (^{34}S) in sulfate (Fig. 4c: phase shift 0–0.8). Fig. 5 shows that the ratios in the amplitudes of the LIP and sulfur isotope cycles are stable at ~600 km^3 LIPs' version #2 related magma production correlates with ~2‰ $\delta^{34}S_{sulfate}$ increase and an average loss of >120 well-dated marine genera. An increased LIPs' version #2 lava production is also related to a drop in $\delta^{34}S_{sulfate}$ by the same amount of ~1‰/600 × 10^3 km^3 over several million years during the last ~135 Ma (Fig. 4c, e). Thus, an extrapolation of k into the early Paleozoic (~520 Ma) suggests LIP's volume amplitudes of ~1200 × 10^3 km^3 at ~3‰ $\delta^{34}S_{sulfate}$ (Fig. 4d) for each 140 and 62 Ma cycle. As Fig. 2 shows, LIP, $^{87}Sr/^{86}Sr$ and $\delta^{34}S_{sulfate}$ records are

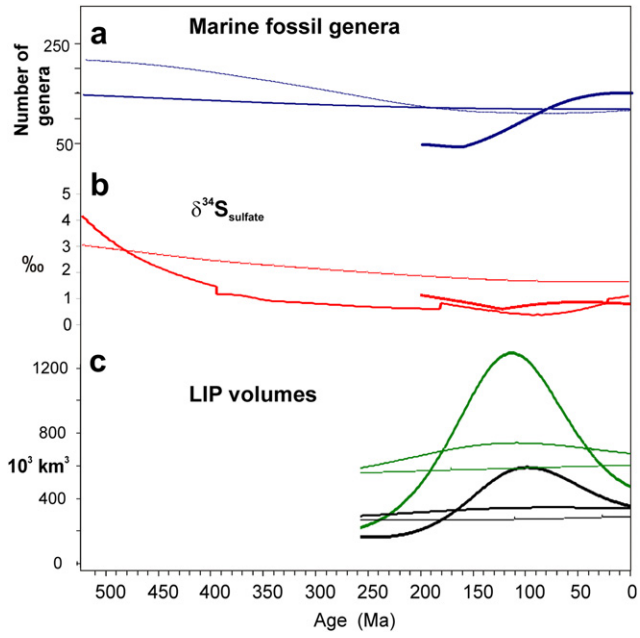

Figure 5. Edge effect corrected amplitudes (wavelet coefficients). a: marine fossil genera (blue); b: $\delta^{34}S_{sulfate}$ (red); c: LIP volumes-version #1 (black), LIP volumes-version #2 (green). Bold line: 28–35 Ma waveband, medium line: 60–70 Ma waveband, thin line: 130–150 Ma waveband. Bottom: Time scale (Gradstein et al., 2005).

well correlated, with the exception of delayed $^{87}Sr/^{86}Sr$ increase during the Silurian–Devonian. Increases of 0.001 $^{87}Sr/^{86}Sr$ correspond to $\delta^{34}S_{sulfate}$ increases of 5‰–15‰, except for the last ~135 Ma when the isotope fluctuations are uncoupled (Fig. 4). Based on the wavebands and amplitude extract by CWT (Figs. 4 and 5), with the assumption that the original LIP volume record in the Paleozoic resembles the Mesozoic/Cenocoic record, the best-fit for LIP volumes (V) would be

$$V = -(350-770)\times10^3 \text{ km}^3 \sin(2\pi t/170 \text{ Ma}) + (300-650)\times10^3 \text{ km}^3 \sin(2\pi t/64.5 \text{ Ma} + 2.3) \quad (7)$$

for t = time in Ma. The ~32 Ma cyclicity is not considered in the reconstruction because of its occurrence only through the last ~135 Ma.

XWT of A10-LIP occurrences with marine genera records shows that almost all cross-variability is concentrated in the 28–35 Ma, 62–65 Ma, and ~140 Ma wavelengths, with a sharp switch from ~62 to ~32 Ma cyclicity at 135 Ma (Fig. 6a). Moreover all signals in these wavelengths are approximately inverted ($-\pi$) between the LIP and other records, i.e. LIP occurrence is linked to marine genera reduction (Fig. 6b). The relationships between LIP occurrences and sulfate isotope records are also concentrated in the 28–35 Ma, 62–65 Ma, and ~140 Ma wavelengths, albeit less dominantly (Fig. 6c). Phase-shifts of ~0 (Fig. 6d) indicate a positive correlation of the ~62 and ~140 Ma signals (Fig. 2), whereas the ~32 Ma cyclicity during the last ~135 Ma is inverse correlated ($-\pi$). It is likely that the high cross-wavelet coefficients between LIP and sulfate isotope records are mostly carried by the LIP variability, because strong cross-wavelet coefficients between marine genera and geochemical records are absent in the ~32 Ma waveband, whereas ~140 and ~62 Ma cycles remain dominant (Fig. 7). The color changes at the ~62 Ma wavelength in the phase parts of the scalograms (Fig. 7b, d, f) indicate that these cycles are not as well correlated between the geochemical records as between the LIP and marine genera records. The yellow color in Fig. 7d indicates a ~+0.5 gradient phase difference between sulfur and strontium isotopes for the ~62 and ~140 Ma cycles, i.e. the $^{87}Sr/^{86}Sr$ isotope increase lags the $\delta^{34}S_{sulfate}$ increase by up to 15 Ma.

In our study, the results of XWT (Eqs. (5) and (6)) have the same uncertainties as CWT as we use the same mother wavelet and parameters for both (see Eqs. (1)–(4)). The multiplication of the individual wavelet coefficients in Eq. (5) reduces the noise level of the cross-modulus (i.e. cross-amplitude) thus highlighting wavelengths that have a high amplitude in both time-series $x(t)$ and $y(t)$. For example, the complete independent cross-amplitude spectra of A10 vs. marine genera and sulfur vs. strontium isotopes (Fig. 6) have very similar temporal extent and relative amplitudes of the ~62 Ma cycle (stronger) and ~140 Ma cycle (weaker). The uncertainty in the phase shift is also linked to the bandwidth and temporal uncertainty (Eqs. (2) and (3)). Test runs using the parameters above on simulations of phase-shifted 140 Ma-sine waves indicate that the uncertainty for a given bandwidth (e.g., 140 ± 5 Ma) is ±0.3 gradients.

5. Discussion

To understand the relation between LIP magmatism and sulfur isotope fluctuations, we have to point out that at present volcanic sulfur contributes 0.33×10^{12} mol/yr with a $\delta^{34}S$ of ~3‰ (Paytan et al., 2004). Currently, sulfur is either deposited to ~45% as sulfide (mostly pyrite) with isotope composition of ~−5‰ to −40‰ or as sulfate with $\delta^{34}S$ of ~+10‰ to +40‰ (Paytan et al., 2004). A marine $\delta^{34}S_{sulfate}$ increase can primarily be the result of (i) lower total sulfur input into the ocean, (ii) increased bacterial sulfide (mostly pyrite) deposition in predominantly anoxic marine basins, and (iii) decreased output from weathering (Paytan et al., 2004). The $^{87}Sr/^{86}Sr$ ratio of marine carbonates reflects primarily the relation between increased oceanic crust production (resulting in low ratios) and increased continental weathering (resulting in high ratios), respectively (Prokoph et al., 2008). Because volcanism is a source and not a sink of sulfur, we interpret the coherency between LIP cyclicity and sulfur isotopes in terms of increased sulfide deposition coeval with increased continental weathering, thus a humid global climate. This process is likely combined with increased shallow water H_2S poisoning, sluggish oceanic circulation, and oceanic anoxia as it has been suggested for some mass-extinctions intervals (Kump et al., 2005). Most Paleozoic extinction events are also associated with fast global sea-level rises, anoxic events and climate warming (Hallam and Wignall, 1999). Thus, we extend the H_2S poisoning hypothesis to all major $\delta^{34}S_{sulfate}$ increases before 200 Ma, and an average marine genera biodiversity loss of ~20 marine genera/+1Δ‰ $\delta^{34}S_{sulfate}$.

During the Jurassic the linkage between LIP-related increased sulfide deposition, weathering and coeval biodiversity weakened. In general the $\delta^{34}S_{sulfate}$ dropped during the Mid-Cretaceous super plume and associated LIP eruptions (Paytan et al., 2004). Possible causes are (i) the total sulfur flux into the ocean has increased by up to 50%, (ii) the sulfate/sulfide fractionation factor decreased globally, (iii) the pyrite deposition rate decreased or (iv) a combination of the three factors (Paytan et al., 2004). Across the Cenomanian–Turonian oceanic anoxic event ~$(0.12–0.36)\times10^3$ Gt sulfur were removed by pyrite burial leading to a +Δ4‰ $\delta^{34}S_{sulfate}$ (Ohkouchi et al., 1999; Turgeon and Creaser, 2008). The CO_2 emissions during the Mid-Cretaceous mantle plume are estimated to account for a 2.8–7.7 °C increase and could have contributed to the long-lasting Mid-Cretaceous warm period (Caldeira and Rampino, 1991). Nevertheless, the oceanic anoxic events during the Mid-Cretaceous super plume were relatively short lived with total of <3 Ma (Leckie et al., 2002) compared to the longevity of Paleozoic oceanic anoxia.

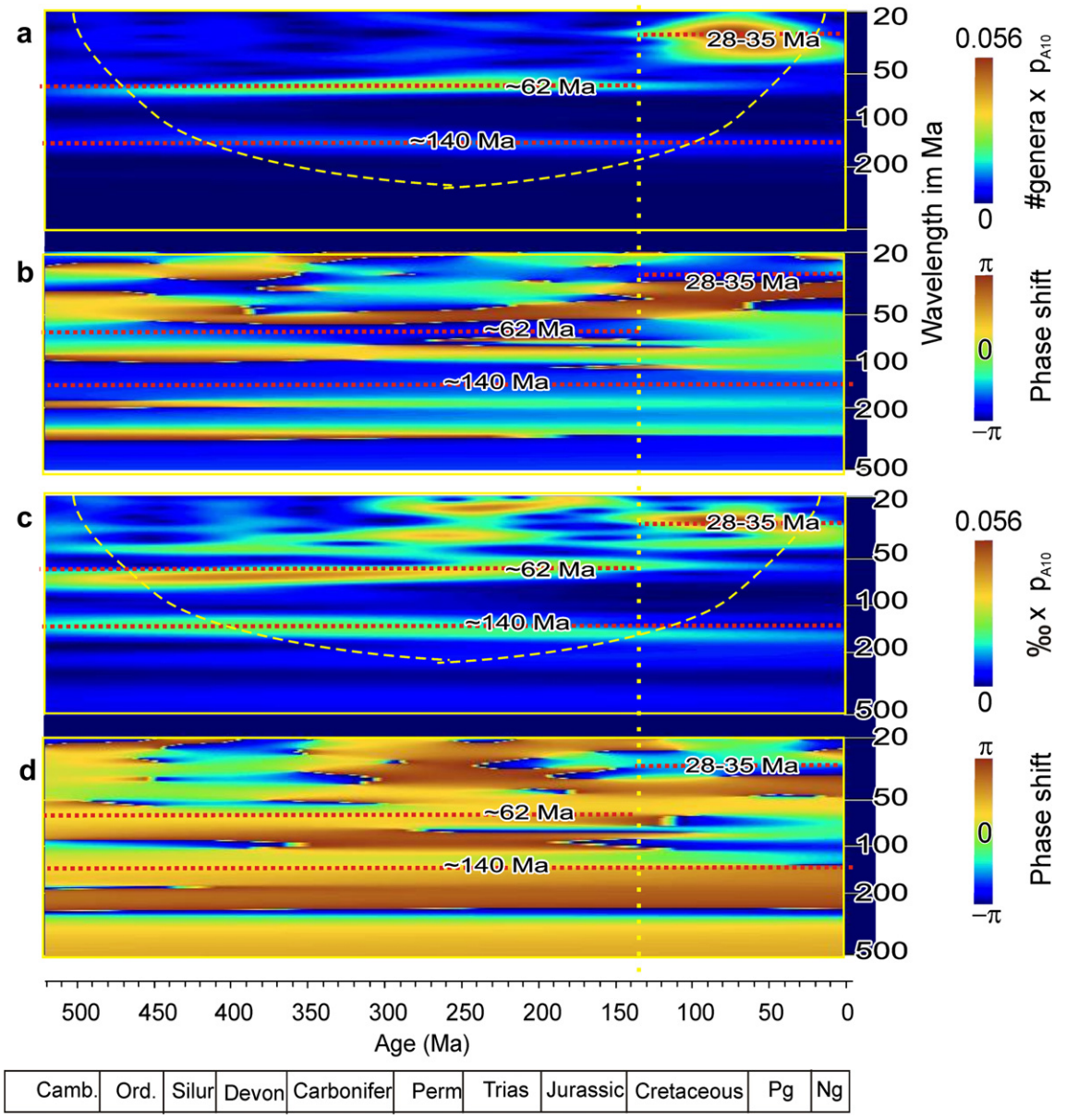

Figure 6. Cross-wavelet analysis of LIP occurrences. a: Cross-wavelet scalogram of LIP_{A10} × # marine genera (Fig. 2a, f); b: phase-shifts between frequencies of LIP_{A10} and # marine genera (Fig. 2a, f); c: cross-wavelet scalogram of $LIP_{A10} \times \delta^{34}S_{sulfate}$ (Fig. 2b, f); d: phase-shifts between frequencies of LIP_{A10} and $\delta^{34}S_{sulfate}$ (Fig. 2b, f). Stripped curves separates frequency–time space of edge effect (Torrence and Compo, 1998) of <20% (above line) from >20% (below line), red dotted lines mark cycle bands, vertical yellow dotted line marks the onset of ~32 Ma cyclicity in LIP and fossil records at ~135 Ma, color code for cross-wavelet coefficient = uncorrected cross-amplitude and phase-shifts on right.

We suggest that the shortness of the anoxic events and the quick recovery of the sulfur and carbon cycles in the last 135 Ma could be due to a more efficient biogeochemical cycling (Ridgwell, 2005), including organic carbon and sulfur storage in the deep-sea instead of in shelf seas. This could lead to the weakening of sulfur isotope and marine biodiversity fluctuation for the last ~135 Ma as shown in Fig. 2.

Thus, the addition of a 28–35 Ma geological cycle and a weakening of the ~62 Ma cycle during the last 135 Ma could be a new nonlinear response of the ocean-atmosphere system to the evolved biogeochemical processes, but this would not explain the coherent changes in the LIP cyclicity over the same time interval. However, the similarity between the phase and magnitude of the 28–35 Ma isotope cycles and the LIP cycles is strong (Figs. 2, 4). As alternative causes, changes at Earth's core mantle boundary such as a thinning of the velocity boundary ("D") layer from ~19 to 12 km thickness, changes in the magma viscosity and/or temperature could change the size and periodicity of the LIP events (Courtillot and Besse, 1987; Courtillot and Olsen, 2007), and eventually trigger marine biogeochemical changes.

We speculate that this rarity of Paleozoic LIPs is at least partially a preservational phenomenon because (i) the recycling of ocean crust with a half-life of ~55 Ma (Veizer and Jansen, 1985) results in the removal of all oceanic LIP volcanic rock remnants older than ~190 Ma. This accounts for ~60% of all LIP's and ~60% of the total LIP volumes in the last 184 Ma; (ii) Phanerozoic sediments with a half-life of ~380 Ma (Veizer and Jansen, 1985) cover major parts of the continents and potentially hide LIPs related volcanic rocks and structures, and (iii) the high amplitudes of the ~62 Ma cycles $\delta^{34}S_{sulfate}$ and $^{87}Sr/^{86}Sr$ cycles suggest high amounts of volcanic sulfur and continental weathering-supporting fluid releases

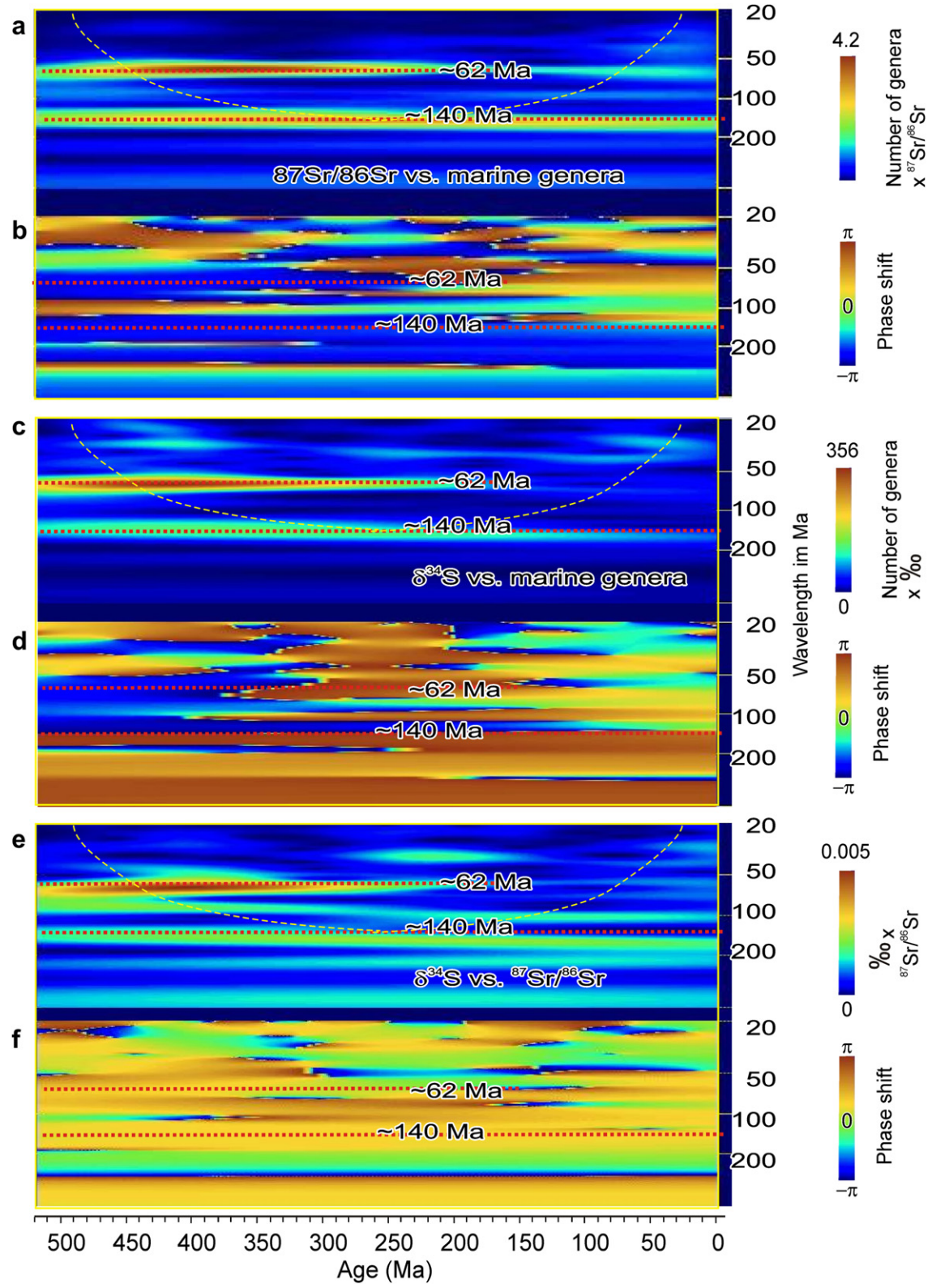

Figure 7. Cross-wavelet analysis: cross-wavelet analysis between marine genera, sulfur and strontium isotope records for the last 520 Ma: a, c, e: modulus (cross-amplitude, no edge effect correction) with color code for cross-amplitude on right side; b, d, f: phase difference with color code for phase shift in gradients on right side. Bottom: Time scale (Gradstein et al., 2005).

(Fig. 2). The LIP record improves for the Precambrian, when more of the sedimentary cover is eroded and roots of LIP's such as dyke swarms are exposed (e.g., Ernst and Buchan, 2001; Ernst and Bleeker, 2010).

LIPs are rarer in the geological record from 270 to 520 Ma and expected LIP's from a modeled ~65 Ma periodicity at ~450 Ma and ~315 Ma are missing (Fig. 2f). Some LIP's during this time interval, such as the Tarim LIP (280 Ma), are currently not included

in the data analysis due to their age uncertainty. Several studies (Young et al., 2009; Buggisch et al., 2010) hint on the possibility of a large and hitherto undetected LIP eruption triggering the Late Ordovician ice age that would explain the drop in the $^{87}Sr/^{86}Sr$ at ~450 Ma (Fig. 2c). The Skagerrak-centered (SC) LIP centered at ~300 Ma has early precursors (Torsvik et al., 2008) that may cover a predicted ~315 Ma LIP event. Data analysis indicates that amplitude of the 62–65 Ma LIP volume cycle is $>600 \times 10^3$ km^3 (Eq. (7)).

The previously noted (Rampino and Stothers, 1988; Prokoph et al., 2004b) ~28–35 Ma cyclicity in geological events and paleoclimate proxies provides only insignificant total variability over the last 520 Ma, but dominates in the last ~200 Ma with sine wave amplitudes equivalent to the 62–65 Ma cyclicity (Fig. 4).

The 140 Ma LIP cyclicity represents the Phanerozoic part of a ~170 Ma (130–190 Ma) LIP cyclicity that is evident for the last 1500 Ma (Prokoph et al., 2004a). The proposed ~140 Ma LIP cycle is coherent with low cosmic ray flux at >95% confidence (Shaviv and Veizer, 2003) as shown in Fig. 2d as well as to the ~140 Ma cycle detected in the oxygen isotope record (Prokoph et al., 2008). Currently, there is no known astrophysical mechanism that can explain the ~140 Ma and 62 Ma sulfur and strontium isotope cyclicity. Thus, for future studies would be interesting to integrate potential galactic and terrestrial long-term driving forces on Earth ocean geochemistry, climate and biodiversity evolution.

6. Conclusion

The study reveals a periodic pattern of large igneous province (LIP) emplacement in comparison with marine isotope records, and quantifies the effects on ocean chemistry and marine biodiversity over the last 520 Ma based on compiled LIP, stable isotope and marine genera record at a data resolution of ~1 Ma.

Time-series analysis using wavelet and cross-wavelet transform does not only show that the ~140 Ma and ~65 Ma cycles are significant in LIP, ocean chemistry and marine biodiversity records throughout the Phanerozoic, but also highlights that a strong ~32 Ma cyclicity in all related records occurs simultaneously at ~135 Ma. The link between LIPs and biodiversity at ~65 Ma periodicity is particularly strong when correlating the volume of the LIPs with the marine genera record. The strong link between oceanic $\delta^{34}S_{sulfate}$ and $^{87}Sr/^{86}Sr$ cycles and LIPs also suggest that several Paleozoic LIPs are not-yet discovered.

Acknowledgments

We thank J. Veizer for discussions, and A. Paytan for providing data. The research was funded by an NSERC discovery grant to AP.

References

Berner, R.A., 2002. Examination of hypothesis for the Permo-Triassic boundary extinction by carbon cycle modeling. Proceedings of the National Academy of Sciences of the United States of America 99, 4172–4177.

Bryan, S.E., Peate, I.U., Peate, D.W., Self, S., Jerram, D.A., Mawby, M.R., Marsh, J.S., Miller, J.A., 2010. The largest volcanic eruptions on Earth. Earth-Science Reviews 102, 207–229.

Buggisch, W., Joachimski, M.M., Lehnert, O., Bergström, S.M., Repetski, J.E., Webers, G.F., 2010. Did intense volcanism trigger the first Late Ordovician icehouse? Geology 38, 327–330.

Caldeira, K., Rampino, M.R., 1993. The aftermath of the K/T boundary mass extinction: biogeochemical stabilization of the carbon cycle and climate. Paleoceanography 8, 515–525.

Caldeira, K., Rampino, M.R., 1991. The mid-Cretaceous superplume, carbon dioxide, and global warming. Geophysical Research Letters 18, 987–990.

Coffin, M.F., Eldholm, O., 1994. Large igneous provinces: crustal structure, dimensions, and external consequences. Review of Geophysics 32, 1–36.

Courtillot, V.E., Renne, P.R., 2003. On the ages of flood basalt events. Comptes Rendus Geoscience 335, 113–140.

Courtillot, V., Besse, J., 1987. Magnetic field reversals, polar wander, and core-mantle coupling. Science 237, 1140–1147.

Courtillot, V., Olsen, P., 2007. Mantle plumes link magnetic superchrons to phanerozoic mass depletion events. Earth and Planetary Science Letters 260, 495–504.

Courtillot, V., Davaille, A., Besse, J., Stock, J., 2003. Three distinct types of hotspots in the Earth's mantle. Earth and Planetary Science Letters 205, 295–308.

Ernst, R.E., Bleeker, W., 2010. Large igneous provinces (LIPs), giant dyke swarms, and mantle plumes: significance for breakup events within Canada and adjacent regions from 2.5 Ga to the present. Canadian Journal of Earth Sciences 47, 695–739.

Ernst, R.E., Buchan, K.L., 2001. Large mafic magmatic events through time and links to mantle-plume heads. Geological Society of America Special Paper 352, 483–575.

Gradstein, F., Ogg, J., Smith, A., 2005. A Geologic Time Scale 2004. Cambridge University Press, Cambridge.

Grinsted, A., Moore, J.C., Jevrejeva, S., 2004. Application of the cross wavelet transform and wavelet coherence to geophysical time series. Nonlinear Processes in Geophysics 11, 561–566.

Hallam, A., Wignall, P.B., 1999. Mass extinctions and sea-level changes. Earth-Science Reviews 48, 217–250.

Isozaki, Y., 2009. Integrated "plume winter" scenario for the double-phased extinction during the Paleozoic–Mesozoic transition: the G-LB and P-TB events from a Panthalassan perspective. Journal of Asian Earth Sciences 36, 459–480.

Jury, M.R., Enfield, D.B., Mélice, J., 2002. Tropical monsoons around Africa: stability of El Niño–Southern Oscillation associations and links with continental climate. Journal of Geophysical Research 107 (C10), 3151–3167.

Kampschulte, A., Strauss, H., 2004. The sulfur isotopic evolution of Phanerozoic seawater based on the analysis of structurally substituted sulfate in carbonates. Chemical Geology 204, 255–286.

Kuiper, K.F., Deino, A., Hilgen, F.J., Krijgsman, W., Renne, P.R., Wijbrans, J.R., 2008. Synchronizing rock clocks of Earth history. Science 320, 500–504.

Kump, L.R., Pavlov, A., Arthur, M.A., 2005. Massive release of hydrogen sulfide to the ocean and atmosphere during intervals of oceanic anoxia. Geology 33, 397–400.

Labat, D., 2005. Recent advances in wavelet analyses: part 1. A review of concepts. Journal of Hydrology 314, 275–288.

Leckie, R.M., Bralower, T.J., Cashman, R., 2002. Oceanic anoxic events and plankton evolution: biotic response to tectonic forcing during the mid-Cretaceous. Paleoceanography 17, 1301–1329.

Maraun, D., Kurths, J., 2004. Cross wavelet analysis: significance testing and pitfalls. Nonlinear Processes in Geophysics 11, 505–514.

Maraun, D., Kurths, J., Holschneider, M., 2007. Nonstationary Gaussian processes in wavelet domain: synthesis, estimation, and significance testing. Physical Review E 75, 016707-1–016707-13.

Melott, A.L., Bambach, R.K., Petersen, K.D., McArthur, J.M., 2012. An ~60-million-year periodicity is common to marine $^{87}Sr/^{86}Sr$, fossil biodiversity, and large-scale sedimentation: what does the periodicity reflect? The Journal of Geology 120, 217–226.

Morlet, J., Arehs, G., Fourgeau, I., Giard, D., 1982. Wave propagation and sampling theory. Geophysics 47, 203–206.

Ohkouchi, N., Kawamura, K., Kajiwara, Y., Wada, E., Okada, M., Kanamatsu, T., Taira, A., 1999. Sulfur isotope records around Livello Bonarelli (northern Apennines, Italy) black shale at the Cenomanian–Turonian boundary. Geology 27, 535–538.

Paytan, A., Kastner, M., Campbell, D., Thiemens, M.H., 2004. Seawater sulfur isotope fluctuations in the Cretaceous. Science 304, 1663–1665.

Prokoph, A., Barthelmes, F., 1996. Detection of nonstationarities in geological time series: wavelet transform of chaotic and cyclic sequences. Computer & Geoscience 22, 1097–1108.

Prokoph, A., Ernst, R.E., Buchan, K.L., 2004a. Time-series analysis of large igneous provinces: 3500 Ma to present. Journal of Geology 112, 1–22.

Prokoph, A., Rampino, M.R., El Bilali, H., 2004b. Periodic components in the diversity of calcareous plankton and geological events over the past 230 Myr. Palaeogeography, Palaeoclimatology, Palaeoecology 207, 105–125.

Prokoph, A., Shields, G.A., Veizer, J., 2008. Compilation and time-series analysis of a marine carbonate $\delta^{18}O$, $\delta^{13}C$, $^{87}Sr/^{86}Sr$ and $\delta^{34}S$ database through Earth history. Earth-Science Reviews 87, 113–133.

Rampino, M.R., Stothers, R.B., 1988. Flood basalt volcanism during the past 250 million years. Science 241, 663–668.

Reichow, M.K., Pringle, M.S., Al'Mukhamedov, A.I., Allen, M.B., Andreichev, V.L., Buslov, M.M., Davies, C.E., Fedoseev, G.S., Fitton, J.G., Inger, S., Medvedev, A.Y., Mitchell, C., Puchkov, V.N., Safonova, I.Y., Scott, R.A., Saunders, A.D., 2009. The timing and extent of the eruption of the Siberian Traps large igneous province: implications for the end-Permian environmental crisis. Earth and Planetary Science Letters 277, 9–20.

Rhode, R.A., Muller, R.A., 2005. Cycles in fossil diversity. Nature 434, 208–210.

Ridgwell, A., 2005. A Mid Mesozoic revolution in the regulation of ocean chemistry. Marine Geology 217, 339–357.

Rioul, O., Vetterli, M., 1991. Wavelets and signal processing. IEEE Special Magazine, 14–38.

Saunders, A., Reichow, M., 2009. The Siberian Traps and the End-Permian mass extinction: a critical review. Chinese Science Bulletin 54, 20–37.

Schaefli, B., Maraun, D., Holschneider, M., 2007. What drives high flow events in the Swiss Alps? Recent developments in wavelet spectral analysis and their application to hydrology. Advances in Water Resources 30, 2511–2525.

Sepkoski, J., 2002. A compendium of fossil animal genera. In: Jablonski, D., Foote, M. (Eds.), Bulletins of American Paleontology, vol. 363. Paleontological Research Institution, Ithaca.

Shaviv, N., Veizer, J., 2003. Celestial driver of Phanerozoic climate. GSA Today 13, 4–10.

Shields, G., Veizer, J., 2002. Precambrian marine carbonate isotope database: version 1.1. Geochemistry, Geophysics, Geosystems 3 (6), 12.

Svensen, H., Planke, S., Polozov, A.G., Schmidbauer, N., Corfu, F., Podladchikov, Y.Y., Jamtveit, B., 2009. Siberian gas venting and the end-Permian environmental crisis. Earth and Planetary Science Letters 277, 490–500.

Torrence, C., Compo, G.P., 1998. A practical guide to wavelet analysis. Bulletin of the American Meteorological Society 79, 61–78.

Torsvik, T.H., Smethurst, M.A., Burke, K., Steinberger, B., 2008. Long term stability in deep mantle structure: evidence from the ~300 Ma Skagerrak-centered large igneous province (the SCLIP). Earth and Planetary Science Letters 267, 444–452.

Turgeon, S.C., Creaser, R.A., 2008. Cretaceous oceanic anoxic event 2 triggered by a massive magmatic episode. Nature 454, 323–326.

Veizer, J., Jansen, S.L., 1985. Basement and sedimentary recycling-2: time dimension to global tectonics. The Journal of Geology 93, 625–643.

Wignall, P.B., 2001. Large igneous provinces and mass extinctions. Earth and Planetary Science Letters 53, 1–33.

Young, S.A., Saltzman, M.R., Kenneth, A., Foland, K.A., Linder, J.S., Kump, L.R., 2009. A major drop in seawater $^{87}Sr/^{86}Sr$ during the Middle Ordovician (Darriwilian): links to volcanism and climate? Geology 37, 951–954.